Journal of Electrical and Computer Engineering Innovations
(JECEI)
Journal homepage: http://www.jecei.sru.ac.ir

Research paper

Experimental Performance of Adaptive Fast Terminal Sliding Mode Control on a Suspended Cable Robot

M. Isaac Hosseini, M. Reza J. Harandi, S.A. Khalilpour, H.D. Taghirad *

Faculty of Electrical Engineering, K. N. Toosi University of Technology, Tehran, Iran.

Article Info

Article History:
Received 15 February 2018
Reviewed 13 April 2018
Revised 23 June 2018
Accepted 01 October 2018

Keywords:
Suspended cable-driven parallel manipulator
Fast terminal sliding mode
Finite-time convergence
Robust control
Adaptive control

*Corresponding Author's Email Address:
taghirad@kntu.ac.ir

Abstract

Background and Objectives: Fast-tracking of reference trajectory and performance improvement in the presence of dynamic and kinematic uncertainties is of paramount importance in all robotic applications. This matter is even more important in the case of cable-driven parallel robots due to the flexibility of the cables. Furthermore, cables are limited in the sense that they can only apply tensile forces, for this reason, feedback control of such robots becomes more challenging than conventional parallel robots.

Methods: To address these requirements for a suspended cable-driven parallel robot, in this paper a novel adaptive fast terminal sliding mode controller is proposed and then the stability of the closed-loop system is proven. In the proposed controller, a nonlinear term as a fractional power term is used to guarantee the convergent response at a finite time.

Results: At last, to show the effectiveness of the proposed controller in tracking the reference trajectory, simulations and the required experimental implementation is performed on a suspended cable-driven robot. This robot, named ARAS-CAM, has three degrees of transmission freedom.

Conclusion: The obtained experimental results confirm the suitable performance of this method for cable robots in the presence of dynamic uncertainties.

Introduction

Cable-driven parallel robots (CDPRs) are a special class of parallel robots and similar to parallel robots where the end-effector's motion is bounded by several closed kinematic chains, cable robots also constrain the motion of the moving platform by several closed chains comprised of cables. Exploiting cables instead of heavy and expensive rigid links brings many advantages to the robot such as high acceleration [1], large workspace [2], and simple structures [3]. These properties make this family of robots suitable choices for real-world applications. From the many scenarios where cable robots have been employed, we can name airplane maintenance facilities [4], video capturing [5], rehabilitation and rescue missions [6].

Cable tension is of paramount importance in CDPRs since cables can only pull the end-effector but not push it. This physical limitation divides this category of robots into two groups; fully constrained and suspended. In fully constrained cable robots, the number of actuators is at least one more than the degrees of freedom (DOF) [7]. Moreover, larger workspaces and optimized performance can be achieved through extra cables. However, in cable–suspended parallel robots (CSPRs), cables are pulled by an external force (passive force). Gravity is an example of a passive force that is used in different structures [8]. However, the control of these robots is much more challenging than conventional

parallel robots due to the replacement of cables rather than the rigid links,as well as the existence of dynamic and kinematic uncertainties [9]-[12]. For this purpose, it is essential to provide a controller that can increase tracking speed while also increase accuracy.

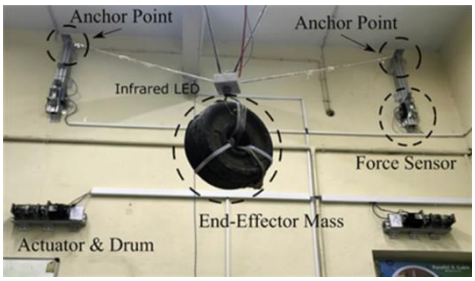

Fig. 1: Prototype of a CSPR with one degree of actuator redundancy called ARAS-CAM

Sliding mode controller (SMC) is one of the most recognized nonlinear and robust controllers due to features such as simple design, robustness, reduced order, and ease of implementation [13]. Due to these suitable properties, it has been applied in many applications in various industries, e.g., robotic manipulators [14], spacecraft [15], and power systems [16]. The main idea of this method is to design a controller that drives the states of the system towards a defined sliding surface. In traditional SMCs though, since the sliding surface is defined to be linear, the asymptotic convergence cannot be achieved in finite time. To solve this problem, a nonlinear term (a fractional power term) is used in the sliding surface [17], through which the convergence of the system to the equilibrium point is guaranteed to happen at a finite time, this procedure is called terminal sliding mode control (TSM). Although TSM has been able to offer better performance, it has challenges such as slow convergence to the origin, when the system is far from the origin, even slower than SMC [18]. For this purpose, Yu and Man proposed the fast terminal sliding mode (FTSM) controller [19]. This method combines the advantages of the TSM control and the SMC so that fast transient convergence both at a distance from and at a close range of the origin can be obtained. The main focus of this paper is to design and implement an adaptive FTSM controller to increase speed and precision of tracking performance in the presence of dynamic uncertainties for a cable robot. Furthermore, the stability of the closed-loop system is proved by the Lyapunov stability theorem, also to demonstrate the effectiveness of the proposed controller, it is implemented on the ARAS-CAM.

The rest of this paper is organized as follows: In Section 2, ARAS-CAM's general structure and characteristics are described. In Section 3, the kinematic and the dynamic modeling of the robot are introduced in detail. The synthesis and design of the proposed controller (adaptive FTSM controller) for the suspended robot are explained in Section 4. Section 5 is dedicated to present the simulation result and experimental performance of the proposed control scheme for the mentioned robot. Finally, Section 6 concludes this paper.

ARAS-CAM Cable-suspended parallel robot

The ARAS–CAM robot is a prototype of a cable-suspended parallel robot (As shown in Fig. 1) in which gravity is used as a passive force to ensure that cables are tensile. In this robot, four actuators have been used to move the end-effector in three degrees of freedom by driving the cables as shown in Fig. 2 (transitional movement on axes x, y, and z). As shown in Fig. 1 and Fig. 2, each cable, on one side, is connected to a common point on the end- effector and the other side, it is connected to the actuator by a guiding pulley and a few other pulleys. Furthermore, to improve the performance of the robot, a load cell as a force sensor in each kinematic chain and a stereo camera modified to be strictly sensitive to IR light as position sensors have been used. A more detailed description of the designed system for the robot is given in [11].

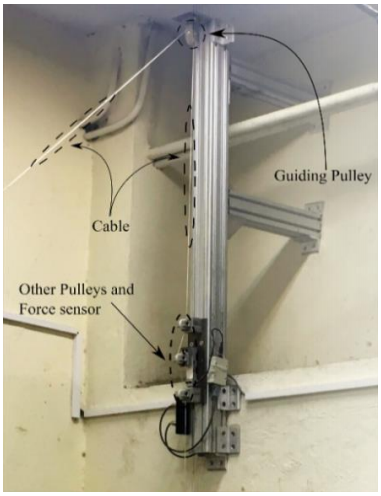

Fig. 2: A part of a kinematic chain of ARAS-CAM robot.

Modeling of ARAS-CAM

A. Kinematic Model

The kinematics notation of the robot aforementioned is shown in [11].

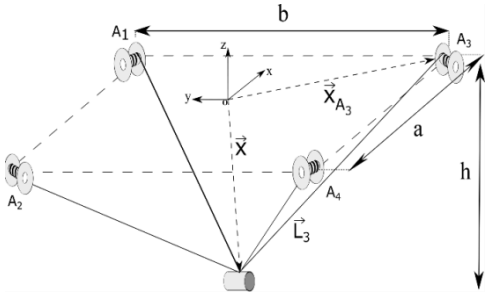

Fig. 3: Schematics of ARAS-CAM cable-driven robot.

In this figure, $\boldsymbol{L}_i$ denotes the vector along $i'th$ cable and A_i denotes anchor points on the XY plane of the coordinate frame $\mathcal{O}$. Constants $a, b,$ and h denote the width, length, and height of the robot's workspace, respectively. The positions of the anchor points and end-effector are represented by vectors $\boldsymbol{X}_{A_i}$ and $\boldsymbol{X}$, respectively. The loop closure relationship for the robot is given as follows

$$\boldsymbol{X} = \boldsymbol{X}_{A_i} + \boldsymbol{L}_i \quad \text{for } i = 1, \dots, 4. \tag{1}$$

Inverse kinematics is derived by rewriting the loop closure relation algebraically as follows

$$\boldsymbol{l_i^2} = \boldsymbol{(X - X_{A_i})^T (X - X_{A_i})}, \tag{2}$$

where l_i is the length of $i'th$ cable. Rewrite (2) into scalar form as:

$$l_i^2 = (x - x_{A_i})^2 + (y - y_{A_i})^2 + (z - z_{A_i})^2. \tag{3}$$

To derive Jacobian matrix, $\boldsymbol{J(X)}$, differentiate (3) with to time as follows

$$\dot{l}_i = \frac{(x - x_{A_i})}{l_i}\dot{x} + \frac{(y - y_{A_i})}{l_i}\dot{y} + \frac{(z - z_{A_i})}{l_i}\dot{z} \tag{4}$$

and rewrite it into matrix form as

$$\boldsymbol{\dot{L} = J(X)\dot{X}} \qquad \boldsymbol{L} = \begin{bmatrix} l_1 \\ l_2 \\ l_3 \\ l_4 \end{bmatrix} \qquad \boldsymbol{X} = \begin{bmatrix} x \\ y \\ z \end{bmatrix}$$

$$\boldsymbol{J(X)} = \begin{bmatrix} \frac{(x - x_{A_1})}{l_1} & \frac{(y - y_{A_1})}{l_1} & \frac{(z - z_{A_1})}{l_1} \\ \frac{(x - x_{A_2})}{l_2} & \frac{(y - y_{A_2})}{l_2} & \frac{(z - z_{A_2})}{l_2} \\ \frac{(x - x_{A_3})}{l_3} & \frac{(y - y_{A_3})}{l_3} & \frac{(z - z_{A_3})}{l_3} \\ \frac{(x - x_{A_4})}{l_4} & \frac{(y - y_{A_4})}{l_4} & \frac{(z - z_{A_4})}{l_4} \end{bmatrix} \tag{5}$$

B. Dynamic Model

Since the mass of the cables and air resistance are extremely smaller than that of other mechanical parts, therefore in this section, we derive dynamic equations of the robot regardless of the mass of the cables and air resistance.

Thus, the dynamic model of the robot can be written in the Cartesian space in the general form as

$$\boldsymbol{M(X)\ddot{X} + C(X, \dot{X})\dot{X} + G(X) = -J(X)^T \tau}$$

$$\boldsymbol{M(X)} = \begin{bmatrix} m & 0 & 0 \\ 0 & m & 0 \\ 0 & 0 & m \end{bmatrix}, \tag{6}$$

$$\boldsymbol{C(X, \dot{X}) = 0}, \qquad \boldsymbol{G(X)} = \begin{bmatrix} 0 \\ 0 \\ mg \end{bmatrix},$$

where $\boldsymbol{M(X)}$ is the inertia matrix, $\boldsymbol{C(X, \dot{X})\dot{X}}$ is vector of Coriolis, and centripetal forces and $\boldsymbol{G(X)}$ the vector of gravitational forces.

Some important properties of dynamic equations of a robot manipulator that will be very crucial to the stability analysis of the proposed controller are as follows [20]

1. $\boldsymbol{M(X)}$ is a symmetric positive definite matrix for all $\boldsymbol{X} \in \boldsymbol{R^3}$.
2. The matrix $\boldsymbol{\dot{M}(X) - 2C(X, \dot{X})}$ is skew-symmetric

$$\boldsymbol{Q^T\big(\dot{M}(X) - 2C(X, \dot{X})\big)Q = 0}, \qquad \forall \boldsymbol{Q} \in \boldsymbol{R^3} \tag{7}$$

3. The dynamic model of ARAS-CAM robot is linear, then, it can be represented in a linear regression form as follow

$$\boldsymbol{M(X)\ddot{X} + C(X, \dot{X})\dot{X} + G(X)} = \boldsymbol{Y_m(\ddot{X}, \dot{X}, X)\theta_m} \tag{8}$$

Controller Design

This section presents the proposed adaptive FTSM control scheme to drive the ARAS-CAM robot. In the proposed controller, reference tracking is done in a finite time by the FTSM part of the controller and improving the tracking performance in the presence of dynamic uncertainties is achieved through the adaptation law. However, before entering the design of the controller, the initial definitions must be expressed. Hence, the concept of terminal sliding mode and fast terminal sliding mode is given below

Lemma 1. Basic concepts on TSM introduced in [21]: Suppose that V(t) is a positive definite continuous function and there exists a real number $\mu > 0$ and $0 < \eta < 1$ such that satisfies the differential inequality as follows

$$\dot{V}(t) \le -\mu V^{\eta}(t), \quad \forall t \ge t_0. \tag{9}$$

Then, for any given t_0, V(t) satisfies the following inequality

$$V^{1-\eta}(t) \le V^{1-\eta}(t_0) - \mu(1 - \eta)(t - t_0), \quad t_0 \le t \le t_1, \tag{10}$$

and

$$V(t) = 0, \quad \forall t \ge t_1 \tag{11}$$

with t_1 given by

$$t_1 = t_0 + \frac{V^{1-\eta}(t_0)}{\mu(1 - \eta)} \tag{12}$$

■

Lemma 2. Basic concepts on FTSM introduced in [19]: Although TSM expresses the convergence of finite time by (12), when the system is far from the origin, the convergence rate is slow. To overcome this problem, the term $-\alpha V^{\beta}(t)$ is added to right-hand side of (9). So, (9) is rewritten as follows:

$$\dot{V}(t) \le -\alpha V^{\beta}(t) - \mu V^{\eta}(t), \quad \forall t \ge t_0 \tag{13}$$

where $\alpha > 0$ is a real number and $\beta \ge 1$ is an odd integer.

Then, V(t) will converge to the origin in finite time for $\beta = 1$

$$t_1 \le t_0 + \frac{1}{\alpha(1 - \eta)}(ln(\alpha V(t_0)^{1-\eta} + \mu) - ln\ \mu) \tag{14}$$

■

Let us consider tracking error as $\tilde{\boldsymbol{X}} = \boldsymbol{X} - \boldsymbol{X}_d$. Now, we define the sliding surface as follows

$$\boldsymbol{s} = \dot{\tilde{\boldsymbol{X}}} + \boldsymbol{\Gamma}_1\tilde{\boldsymbol{X}} + \boldsymbol{\Gamma}_2\tilde{\boldsymbol{X}}^p, \tag{15}$$

in which $\boldsymbol{\Gamma}_1$, $\boldsymbol{\Gamma}_2$ are positive definite diagonal matrices and $p > 1/2$. Sliding surface proposed in (15) may be interpreted as a velocity error term

$$\boldsymbol{s} = \dot{\boldsymbol{X}} - \dot{\boldsymbol{X}}_r, \tag{16}$$

where $\dot{\boldsymbol{X}}_r = \dot{\boldsymbol{X}}_d - \boldsymbol{\Gamma}_1\tilde{\boldsymbol{X}} - \boldsymbol{\Gamma}_2\tilde{\boldsymbol{X}}^p$, $\ddot{\boldsymbol{X}}_r = \ddot{\boldsymbol{X}}_d - \boldsymbol{\Gamma}_1\dot{\tilde{\boldsymbol{X}}} - p\boldsymbol{\Gamma}_2 diag\left(\begin{bmatrix}\tilde{X}_1^{p-1} & \tilde{X}_2^{p-1} & \tilde{X}_3^{p-1}\end{bmatrix}\right)\dot{\tilde{\boldsymbol{X}}}$. Then, as $\tilde{\boldsymbol{X}} \to \boldsymbol{0}$, $\dot{\boldsymbol{X}}_r \to \dot{\boldsymbol{X}}_d$, hence $\boldsymbol{X}_r$ is called the reference trajectory.

Define the A-FTSM control law as

$$\begin{aligned}\boldsymbol{\tau} &= -\boldsymbol{J}(\boldsymbol{X})^{\dagger}\left(\widehat{\boldsymbol{M}}\ddot{\boldsymbol{X}}_r + \widehat{\boldsymbol{G}} - \boldsymbol{K}_1\boldsymbol{s}^{\boldsymbol{\alpha}_1} - \boldsymbol{K}_2\boldsymbol{s}^{\boldsymbol{\alpha}_2}\right)\\ &= -\boldsymbol{J}(\boldsymbol{X})^{\dagger}\left(\boldsymbol{Y}(\ddot{\boldsymbol{X}}_r)\hat{\theta}_m - \boldsymbol{K}_1\boldsymbol{s}^{\boldsymbol{\alpha}_1} - \boldsymbol{K}_2\boldsymbol{s}^{\boldsymbol{\alpha}_2}\right),\end{aligned} \tag{17}$$

where $\boldsymbol{J}(\boldsymbol{X})^{\dagger} = \boldsymbol{J}(\boldsymbol{X})\left(\boldsymbol{J}(\boldsymbol{X})^T\boldsymbol{J}(\boldsymbol{X})\right)^{-1}$ is the right pseudo-inverse of Jacobian matrix $\boldsymbol{J}(\boldsymbol{X})$, $\widehat{\boldsymbol{M}}$ and $\widehat{\boldsymbol{G}}$ are the estimate of $\boldsymbol{M}$ and $\boldsymbol{G}$, respectively. $(\boldsymbol{K}_1, \boldsymbol{K}_2)$ are positive definite diagonal matrices, $\alpha_1 \geq 1$ is an odd integer and $0 < \alpha_2 < 1$ is the ratio of two odd integers. The regressor form is equal to

$$\boldsymbol{Y}(\ddot{\boldsymbol{X}}_r)\hat{\theta}_m = \begin{bmatrix}\ddot{X}_{r1}\\ \ddot{X}_{r2}\\ \ddot{X}_{r3} + g\end{bmatrix}\hat{m} \tag{18}$$

and adaption law is as follows

$$\dot{\hat{\theta}}_m = -\frac{\boldsymbol{s}^T\boldsymbol{Y}(\ddot{\boldsymbol{X}}_r)}{\gamma}. \tag{19}$$

The proposed control scheme is shown in Fig. 4.

Theorem. Consider dynamics equation (6) for the robot mentioned, the control law (17) and the adaptation law (19).

Then, $\tilde{\mathbf{X}}_{\mathrm{r}}$ converges to zero in finite time.

Proof. Substitute the control law (17) in dynamics equation (6):

$$\begin{aligned}&\boldsymbol{M}(\boldsymbol{X})\ddot{\boldsymbol{X}} + \boldsymbol{C}(\boldsymbol{X}, \dot{\boldsymbol{X}})\dot{\boldsymbol{X}} + \boldsymbol{G}(\boldsymbol{X}) =\\ &-\boldsymbol{J}(\boldsymbol{X})^T\left(-\boldsymbol{J}(\boldsymbol{X})^{\dagger}\left(\widehat{\boldsymbol{M}}\ddot{\boldsymbol{X}}_r + \widehat{\boldsymbol{G}} - \boldsymbol{K}_1\boldsymbol{s}^{\boldsymbol{\alpha}_1}\right.\right.\\ &\left.\left. - \boldsymbol{K}_2\boldsymbol{s}^{\boldsymbol{\alpha}_2}\right)\right)\\ &= \boldsymbol{Y}(\ddot{\boldsymbol{X}}_r)\hat{\theta}_m - \boldsymbol{K}_1\boldsymbol{s}^{\boldsymbol{\alpha}_1} - \boldsymbol{K}_2\boldsymbol{s}^{\boldsymbol{\alpha}_2}.\end{aligned} \tag{20}$$

Then, add $-\boldsymbol{Y}(\ddot{\boldsymbol{X}}_r)\theta_m = -\boldsymbol{M}\ddot{\boldsymbol{X}}_r - \boldsymbol{G}$ to both side of (20):

$$\begin{aligned}\boldsymbol{M}(\ddot{\boldsymbol{X}} - \ddot{\boldsymbol{X}}_r) &= \boldsymbol{M}\dot{\boldsymbol{s}}\\ &= \boldsymbol{Y}(\ddot{\boldsymbol{X}}_r)\tilde{\theta}_m - \boldsymbol{K}_1\boldsymbol{s}^{\boldsymbol{\alpha}_1} - \boldsymbol{K}_2\boldsymbol{s}^{\boldsymbol{\alpha}_2},\end{aligned} \tag{21}$$

in which $\tilde{\theta}_m = \hat{\theta}_m - \theta_m$.

Now consider the following Lyapunov function

$$V = \frac{1}{2}\boldsymbol{s}^T\boldsymbol{M}\boldsymbol{s} + \frac{1}{2}\gamma\tilde{\theta}_m^2, \tag{22}$$

differentiate V with respect to time,

$$\dot{V} = \boldsymbol{s}^T\boldsymbol{M}\dot{\boldsymbol{s}} + \gamma\tilde{\theta}_m\dot{\hat{\theta}}_m, \tag{23}$$

by replacing $\boldsymbol{M}\dot{\boldsymbol{s}}$ from (21) and keeping in mind that θ is constant, one may obtain the following equation

$$\begin{aligned}\dot{V} &= \boldsymbol{s}^T\left(\boldsymbol{Y}(\ddot{\boldsymbol{X}}_r)\tilde{\theta}_m - \boldsymbol{K}_1\boldsymbol{s}^{\boldsymbol{\alpha}_1} - \boldsymbol{K}_2\boldsymbol{s}^{\boldsymbol{\alpha}_2}\right)\\ &\quad + \gamma\tilde{\theta}_m\dot{\hat{\theta}}_m\\ &= -\boldsymbol{s}^T\boldsymbol{K}_1\boldsymbol{s}^{\boldsymbol{\alpha}_1} - \boldsymbol{s}^T\boldsymbol{K}_2\boldsymbol{s}^{\boldsymbol{\alpha}_2}\\ &\quad + \left(\boldsymbol{s}^T\boldsymbol{Y}(\ddot{\boldsymbol{X}}_r) + \gamma\dot{\hat{\theta}}_m\right)\tilde{\theta}_m\end{aligned} \tag{24}$$

by adaptation law (19), $\dot{V}$ is equal to

$$\dot{V} = -\boldsymbol{s}^T\boldsymbol{K}_1\boldsymbol{s}^{\boldsymbol{\alpha}_1} - \boldsymbol{s}^T\boldsymbol{K}_2\boldsymbol{s}^{\boldsymbol{\alpha}_2}. \tag{25}$$

Considering Theorem 1 in [22], it can be shown that the sliding surface $\boldsymbol{s}$ converges to zero in finite time with the upper bound T according to lemma 1 as follows

$$T \leq t_0 + \frac{\max\left(s^{1-\alpha_2}(t_0)\right)}{(1-\alpha_2)k_2^*}, \tag{26}$$

in which k_2^* is the minimum element of $\boldsymbol{K}_2$.

On the sliding surface ($\boldsymbol{s} = 0$), the equation of motion of the robot reduces to $\dot{\tilde{\boldsymbol{X}}} + \boldsymbol{\Gamma}_1\tilde{\boldsymbol{X}} + \boldsymbol{\Gamma}_2\tilde{\boldsymbol{X}}^p = 0$, again, consider lemma 1 and lemma 2. Upper bound for convergence time of $\boldsymbol{X}$ to $\boldsymbol{X}d$ is

$$T' \leq \frac{\max\left(\tilde{\boldsymbol{X}}^{1-p}(T)\right)}{(1-p)\gamma_2^*} \tag{27}$$

in which γ_2^* is the minimum element of $\boldsymbol{\Gamma}_2$. ■

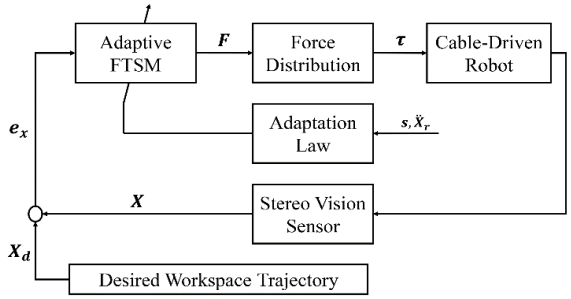

Fig. 4: The proposed control scheme.

Remark 1. Notice that $\ddot{\boldsymbol{X}}_r$ on the sliding surface $\boldsymbol{s} = 0$ is equal to

$$\begin{aligned}&\ddot{\boldsymbol{X}}_r = \ddot{\boldsymbol{X}}_d - \boldsymbol{\Gamma}_1\dot{\tilde{\boldsymbol{X}}}\\ &-p\boldsymbol{\Gamma}_2 diag\left(\begin{bmatrix}\tilde{X}_1^{p-1} & \tilde{X}_2^{p-1} & \tilde{X}_3^{p-1}\end{bmatrix}\right)\dot{\tilde{\boldsymbol{X}}}\\ &= \ddot{\boldsymbol{X}}_d + \boldsymbol{\Gamma}_1\left(\boldsymbol{\Gamma}_1\tilde{\boldsymbol{X}} + \boldsymbol{\Gamma}_2\tilde{\boldsymbol{X}}^p\right)\\ &+ p\boldsymbol{\Gamma}_2 diag\left(\begin{bmatrix}\tilde{X}_1^{p-1} & \tilde{X}_2^{p-1} & \tilde{X}_3^{p-1}\end{bmatrix}\right)\left(\boldsymbol{\Gamma}_1\tilde{\boldsymbol{X}}\right.\\ &\left.+ \boldsymbol{\Gamma}_2\tilde{\boldsymbol{X}}^p\right)\\ &= \ddot{\boldsymbol{X}}_d - \boldsymbol{\Gamma}_1^2\tilde{\boldsymbol{X}} + (1+p)\boldsymbol{\Gamma}_1\boldsymbol{\Gamma}_2\tilde{\boldsymbol{X}}^p\\ &+p\boldsymbol{\Gamma}_2\tilde{\boldsymbol{X}}^{2p-1}.\end{aligned} \tag{28}$$

Therefore, p should be chosen larger than $1/2$ to ensure the boundedness of $\ddot{\boldsymbol{X}}_r$.

Remark 2. It is obvious from (26) and (27) that to reduce the convergence time, the gains $\boldsymbol{\Gamma}_2$ and $\mathbf{K}_2$ shall increase. Furthermore, as explained in lemma 2, by increasing $\mathbf{K}_1, \boldsymbol{\Gamma}_1$ the solution leads to faster convergence.

Results and Discussion

In this section, first, a brief description of the experimental setup is given to implement the proposed controller scheme (shown in Fig. 4), then to demonstrate the effectiveness of the proposed controller, simulations

are conducted on the robot and finally, the results of the implementation indicate applicability of the proposed control algorithm on the ARAS-CAM cable-suspended parallel robot that its specification given in Table 1 and Table 2.

A. Experimental setup

This manipulator has four AC-servo motors that directly coupled to the cables through a drum mechanism. The maximum torque of these motors is $24.4\ kg.cm$ which can apply force Equal to $80N$ to the cables. Also, each actuator is equipped with a non-contact incremental optical encoder providing a total number of 20000 pulses per revolution.

Table 1: Kinematic and Dynamic Parameters of ARAS-CAM

Parameter	Symbol	Value
End-effector mass	m	$4.5\ Kg$
End-effector inertia	I	$\cong 0\ Kg.m^2$
Gear ratio	N	1
Gravity Acceleration	g	$9.8\ m/s^2$
Drum radius	r	$3.5\ cm$
Width	a	$3.56\ m$
Length	b	$7.05\ m$
Height	h	$4.26\ m$

Table 2: Position of the Anchor Points

$A_i's$	Position
1	$(+3.56/2\ ,+7.05/2,0)$
2	$(-3.56/2\ ,+7.05/2,0)$
3	$(+3.56/2\ ,-7.05/2,0)$
4	$(-3.56/2\ ,-7.05/2,0)$

For implementing the proposed control algorithm, we have exploited the power of $MATLAB$ Simulink Real-Time target. The Simulink Real-Time Kernel is a lightweight real-time operating system that is bootable on a conventional X86 PC. After being booted, the kernel establishes an Ethernet link to a host PC with $MATLAB$ software installed on it. Through this link, different Simulink models can be transferred to the kernel to be executed in real-time.

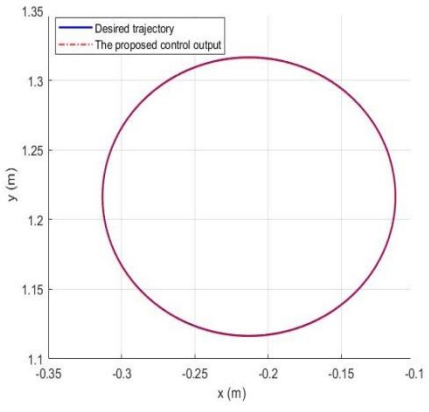

Fig. 5: Simulation results showing the desired path compared to the tracked path by end-effector in (x, y) plane.

Therefore, using this paradigm we can rapidly design our control algorithms and seamlessly deploy them to be evaluated which in turn expedites the design iterations. It is important to note that the model connects to the physical world through data acquisition (DAQ) cards which are represented by specific blocks in the Simulink model. As a position sensor, a modified stereo camera is used. This subsystem receives captured frames of resolution 640 x 480 pixels at a rate of 100 Hz. For localization, an infrared LED that is embedded on the top of the end-effector is detected by the aforementioned vision subsystem which is installed on the top of the robot's workspace. Thereafter, by performing some geometrical transformations, coordinate systems of the vision subsystem and the robot are co-registered.

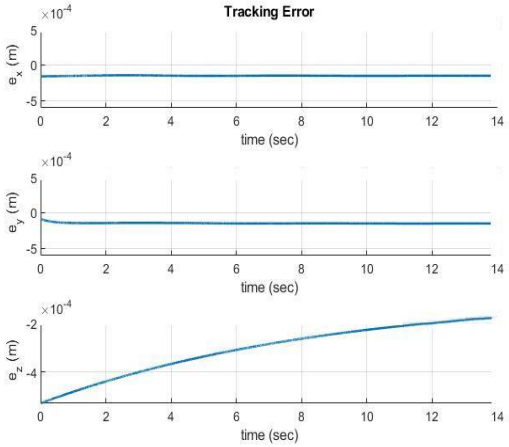

Fig. 6: Simulation results showing position tracking error in all directions.

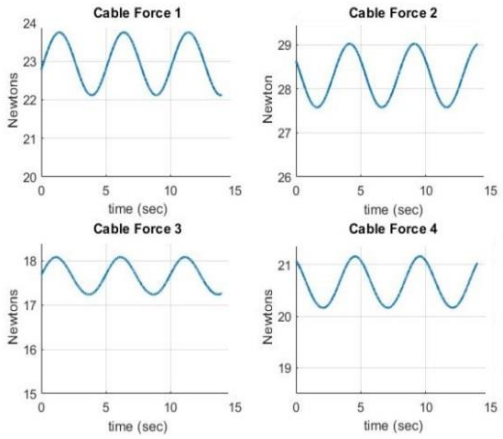

Fig. 7: Simulation results showing tension changes in the cables.

As previously noted, cable tension is of paramount importance in cable-driven parallel robots. For this reason, the algorithm used for force distribution in the proposed control scheme (As shown in Fig. 4) is similar to the method described in detail in [11], which ensures all the cables in the feasible workspace of the robot are under tension. Furthermore, the reference trajectory is designed to maneuver the robot within a feasible

workspace [23] to ensure that the cable forces remain positive with the method mentioned in the entire trajectory.

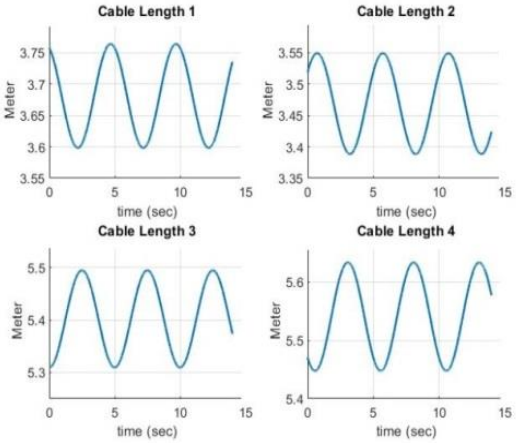

Fig. 8: Simulation results showing measured cable length variation during robot movement.

B. Simulation Result

The parameters required for the proposed controller in the simulation are selected as follows

$\alpha_1 = 1$ $\alpha_2 = 9/11$ $p = 9/11$
$\boldsymbol{\Gamma}_1 = 100\, \boldsymbol{I}_{3\times3}$ $\boldsymbol{\Gamma}_2 = 20\, \boldsymbol{I}_{3\times3}$
$\boldsymbol{K}_1 = 100\, \boldsymbol{I}_{3\times3}$ $\boldsymbol{K}_2 = 20\, \boldsymbol{I}_{3\times3}$

The intended path to simulate the movement of the end-effector in the Cartesian space is a circular trajectory with a radius of 20 cm on the (X, Y) plane, which is performed after the robot arrives at a specific height. Note that the desired velocity and acceleration of the trajectory at initial and final time is zero. Also, it is assumed that the precise knowledge of the mass of the end-effector and the friction parameters of the actuators are not known (both in simulation and in implementation). Fig. 5 shows the reference and actual circle at a constant height. As this figure shows the proposed controller provides a suitable performance in the presence of dynamic uncertainties. Furthermore, Fig. 6 illustrates the error rate more accurately in all three directions that the errors are very small and circa 10^{-4}. Moreover, Fig. 7 shows the tension of the cables which are all positive during the robot movements. Cable length changes are also shown in Fig. 8. Its sinusoidal changes are also due to the circular path which it is designed for them.

C. Experimental Result

In simulations, many effective factors such as noise, actuator dynamics, very small delays, etc. are not considered, and on the other hand, it is assumed that system information is fully available.

Due to these reasons, the results of implementations are not always the same as simulation results. Although ARAS-CAM robot also suffered from these factors, experimental results show that the proposed controller can provide suitable performance in the presence of these factors.

The reference trajectory designed for the robot, like the previous subsection, is a circle on the (X, Y) plane at a constant height. With the exception that the circle radius has doubled in this scenario (40cm). The controller gains are also selected in such a way that they can ensure closed-loop system stability and proper tracking performance for the whole maneuver.

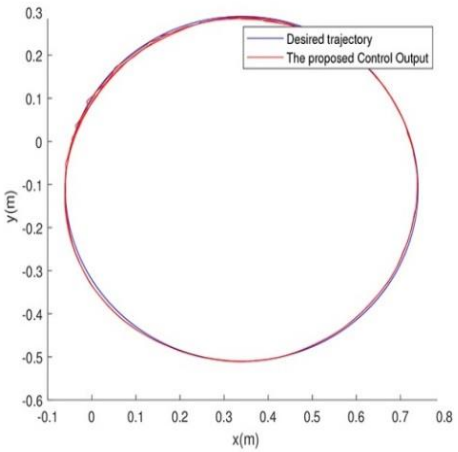

Fig. 9: Implementation results showing the actual and desired position of the end-effector.

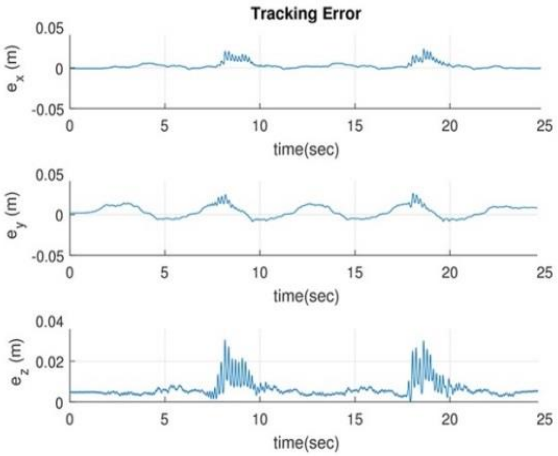

Fig. 10: Implementation results showing position tracking error in all directions.

Controller gains are in this experiment as

$\alpha_1 = 1$ $\alpha_2 = 7/9$ $p = 7/9$
$\boldsymbol{\Gamma}_1 = 80\, \boldsymbol{I}_{3\times3}$ $\boldsymbol{\Gamma}_2 = 7\, \boldsymbol{I}_{3\times3}$
$\boldsymbol{K}_1 = 70\, \boldsymbol{I}_{3\times3}$ $\boldsymbol{K}_2 = \boldsymbol{I}_{3\times3}$

Fig. 9 shows the tracking performance of the robot with the assumption that the mass of the end-effector is unknown.

As it is observed, the robot is capable to follow the reference trajectory by using the A-FTSM controller. Furthermore, Fig. 10 illustrates the tracking errors, which

are less than two centimeters in the worst case in all directions.

Fig. 11 shows that the force distribution used in this experiment provides the necessary tension for all cables during the movement. Also, the sinusoidal changes of the cables in the last figure (Fig. 12) indicate a reference circular trajectory for the ARAS-CAM robot.

Conclusion

Tracking of the reference trajectory at high speed and precision in the cable robots is much more challenging than conventional parallel robots due to the replacement of cables rather than the rigid links. For this purpose, in this paper, an adaptive controller based on FTSM has been proposed for a cable-suspended parallel robot known as ARAS-CAM.

For this purpose, kinematics and dynamics of the robot were first described, then after the introduction of TSM and FTSM, the proposed controller was presented in this section.

In the next section, the stability of the closed-loop system in the presence of dynamic uncertainties was proved based on the Lyapunov stability theory, so that the proposed controller can produce a suitable performance.

To demonstrate the effectiveness of the proposed controller, at first, simulations were performed on MATLAB software, then to evaluate the applicability of the proposed controller, real-time experiments were conducted on ARAS-CAM robot.

The experimental results have shown that the performance of the proposed controller in the presence of dynamic uncertainties is very acceptable.

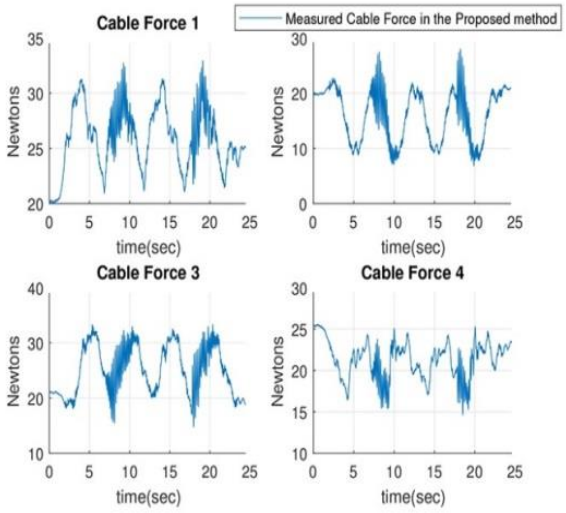

Fig. 11: Implementation results showing the tension of the cables during the execution of a circular trajectory.

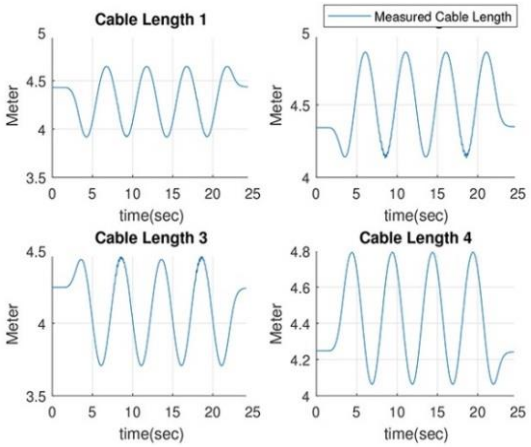

Fig. 12: Implementation results showing cables length variation.

Author Contributions

M. Isaac Hosseini is the main author of the manuscript, also he and S. Ahmad Khalilpour have designed and implemented the experiments. M. Reza J. Harandi examined the proposed controller theoretically and proved the stability of the closed-loop system. Hamid D. Taghirad is also the supervisor of this group and the main and final editor of the manuscript.

Acknowledgment

The authors gratefully acknowledge R. Khorrambakhat and N. Khodadadi for guiding and help to finish this manuscript.

Conflict of Interest

The author declares that there is no conflict of interests regarding the publication of this manuscript. In addition, the ethical issues, including plagiarism, informed consent, misconduct, data fabrication and/or falsification, double publication and/or submission, and redundancy have been completely observed by the authors.

Abbreviations

X	Position of the end effector
X_{Ai}	Position of the anchor point
L	Cable length
$J(X)$	Jacobian matrix
$M(X)$	Inertia matrix
$C(X,\dot{X})$	Coriolis term
$G(X)$	Gravitational vector
τ	Force of cables
$Y_m(\ddot{X},\dot{X},X)$	linear regression of dynamic model
θ_m	Parameters of dynamic model
s	Sliding surface
$\tilde{X}$	Tracking error
g	Gravity Acceleration
m	End-effector mass

References

[1] S. Kawamura, H. Kino, C. Won, "High-speed manipulation by using parallel wire-driven robots," Robotica, 18(3): 13-21, 2000.

[2] H. D. Taghirad, M. Nahon,Kinematic, "Dynamic analysis of a macro-micro redundantly actuated parallel manipulator," Advanced Robotics, 22(6-7): 657-87, 2008.

[3] S. A. Khalilpour, R. Khorrambakht, H. D. Taghirad, P. Cardou, "Wave based control of a deployable cable driven robot" in Proc. 6th RSI International Conference on Robotics and Mechatronics (IcRoM): 166-171, 2018.

[4] D. Q. Nguyen, M. Gouttefarde, O. Company, F. Pierrot, "On the analysis of large-dimension reconfigurable suspended cable-driven parallel robots," in Proc. The IEEE International Conference on Robotics and Automation): 5728–5735, 2014.

[5] L. Cone, Skycam: An aerial robotic camera system. Byte, 10: 122132, 1985.

[6] J. Lenarcic, M. Stanisic, Advances in Robot Kinematics: Motion in Man and Machine, 2010.

[7] R. Verhoeven, M. Hiller, S. Tadokoro, "Workspace, stiffness, singularities and classification of tendon-driven Stewart platforms," Advances in Robot Kinematics: Analysis and Control: 105–114, 1998.

[8] R. Bostelman, J. Albus, N. Dagalakis, A. Jacoff, J. Gross, "Applications of the NIST robocrane," in Proc. The 5th International Symposium on Robotics and Manufacturing: 14–18, 1994.

[9] S. Khalilpour, R. Khorrambakht, M. Harandi, H. D. Taghirad, P. Cardou, "Robust dynamic sliding mode control of a deployable cable driven robot," in Proc. Iranian Conference on Electrical Engineering (ICEE): 863–868, 2018.

[10] S. Qian, B. Zi, H. Ding, "Dynamics and trajectory tracking control of cooperative multiple mobile cranes," Nonlinear Dynamics, 83(1-2): 89–108, 2016.

[11] S. A. Khalilpour, R. Khorrambakht, H. D. Taghirad, P. Cardou, "Robust cascade control of a deployable cable-driven robot," Journal of Mechanical Systems and Signal Processing, 127: 513-530, 2019.

[12] R. Babaghasabha, M. A. Khosravi, H. D. Taghirad, "Adaptive control of KNTU planar cable-driven parallel robot with uncertainties in dynamic and kinematic parameters," Cable-Driven Parallel Robots: 145–159, 2015.

[13] S. Ding, S. Li, W. X. Zheng, "Brief paper: new approach to second order sliding mode control design," IET Control Theory & Applications, 7(18): 2188–2196, 2013.

[14] T.-H. S. Li, Y.-C. Huang, "MIMO adaptive fuzzy terminal sliding mode controller for robotic manipulators," Information Sciences, 180(23): 4641–4660, 2010.

[15] Z. Song, H. Li, K. Sun, "Finite-time control for nonlinear spacecraft attitude based on terminal sliding mode technique," ISA Transactions, 53(1): 117–124, 2014.

[16] G. Yang, Y. Jia, M. Qin, Y. Fang "Research of low voltage shore power supply used on shipping based on sliding control," Journal of Electrical and Computer Engineering Innovations, 5(2): 101-108, 2017.

[17] M. Keshavarz, M. H. Shafiei, "Design of a novel framework to control nonlinear affine systems based on fast terminal sliding mode controller," Journal of Electrical and Computer Engineering Innovations, 5(2): 101-108, 2017.

[18] Y. Wu, B. Wang, G. Zong, "Finite-time tracking controller design for nonholonomic systems with extended chained form," IEEE Transactions on Circuits and Systems II: Express Briefs, 52(11): 798–802, 2005.

[19] X. Yu, M. Zhihong, "Fast terminal sliding-mode control design for nonlinear dynamical systems," IEEE Transactions on Circuits and Systems I: Fundamental Theory and Applications, 49(2): 261–264, 2002.

[20] H. D. Taghirad, Parallel robots: mechanics and control. CRC press, 2013.

[21] K. Saoudi, M. Harmas, "Enhanced design of an indirect adaptive fuzzy sliding mode power system stabilizer for multi-machine power systems," International Journal of Electrical Power & Energy Systems, 54: 425–431, 2014.

[22] S. Yu, G. Guo, Z. Ma, J. Du, "Global fast terminal sliding mode control for robotic manipulators," International Journal of Modelling, Identification and Control, 1(1): 72–79, 2006.

[23] M. Gouttefarde, J.-P. Merlet, D. Daney, "Wrench-feasible workspace of parallel cable-driven mechanisms," in Proc. 2007 IEEE International Conference on Robotics and Automation): 1492–1497, 2007.

Biographies

Mohammad Isaac Hosseini received the B.Sc. degree in Electrical Engineering from Qom University of Technology, Qom, Iran, in 2017. He is currently a master's student in the field of Control Engineering at K.N. Toosi University, Tehran, Iran. His research interests are study and analysis of nonlinear systems and control of parallel robots with particular emphasis on cable-driven robots.

Mohammad Reza Jafari Harandi has received his B.Sc. and M.Sc. degrees in Control Engineering from Sharif University, Tehran, Iran, in 2014 and 2016, respectively. He is currently pursuing a Ph.D. in Control Engineering at K.N. Toosi University, Tehran, Iran. His current research interests include various aspects including control of under-actuated robots, nonholonomic systems, and cable-driven robots.

Seyed Ahmad Khalilpour has received his B.Sc. degree in Telecommunication Engineering from Shahed University, Tehran, Iran, in 2010, his M.Sc. in Mechatronic Engineering in 2013 from K.N. Toosi University, Tehran, Iran. He is currently pursuing a Ph.D. in Control Engineering at K.N. Toosi University, Tehran, Iran. His current research interests include various aspects of dynamics and control of parallel robots with particular emphasis on cable-driven robots.

Hamid D. Taghirad received the B.Sc. degree in Mechanical Engineering from Sharif University of Technology, Tehran, Iran, in 1989 and the M.Sc. degree in Mechanical Engineering and the Ph.D. degree in Electrical Engineering from McGill University, Montreal, QC, Canada, in 1993 and 1997, respectively. He is currently a Professor and the Dean of Faculty of Electrical Engineering, Department of Systems and Control and the Director of the Advanced Robotics and Automated System, K.N. Toosi University of Technology, Tehran, Iran. His publications include five books and more than 190 papers in international journals and conference proceedings. His research interests include robust and nonlinear control applied to robotic systems. Dr. Taghirad is the Chairman of the IEEE control system chapter in the Iran section, a member of the board of the Industrial Control Center of Excellence, K. N. Toosi University of Technology. His research interest includes robust and nonlinear control applied to robotic systems.

How to cite this paper:
M. Isaac Hosseini, M. Reza J. Harandi, S. A. Khalilpour, H. D. Taghirad, "Experimental Performance of Adaptive Fast Terminal Sliding Mode Control on A Suspended Cable Robot," Journal of Electrical and Computer Engineering Innovations, 7(1): 59-67, 2019.

DOI: 10.22061/JECEI.2019.5669.244

URL: http://jecei.sru.ac.ir/article_1172.html